Effect of surface roughness on fouling of RO and NF membranes during filtration of a high organic surficial groundwater

Colin Hobbs, Seungkwan Hong and James Taylor

ABSTRACT

Fouling characteristics of various thin film composite polyamide reverse osmosis (RO) and nanofiltration (NF) membranes were systematically investigated using a high organic surficial groundwater obtained from the City of Plantation, Florida. Prior to bench-scale fouling experiments, surface properties of the selected RO and NF membranes were carefully analysed in order to correlate the rate and extent of fouling to membrane surface characteristics, such as roughness, charge and hydrophobicity. More specifically, the surface roughness was characterized by atomic force microscopy, while the surface charge and hydrophobicity of the membranes were evaluated through zeta potential and contact angle measurements, respectively. The results indicated that membrane fouling became more severe with increasing surface roughness, as measured by the surface area difference, which accounts for both magnitude and frequency of surface peaks. Surface roughness was correlated to flux decline; however, surface charge was not. The limited range of hydrophobicity of the flat sheet studies prohibited conclusions regarding the correlation of flux decline and hydrophobicity.

Key words | hydrophobicity, membrane fouling, nanofiltration, reverse osmosis, surface charge, surface roughness

Colin Hobbs (corresponding author)
James Taylor
Civil and Environmental Engineering Department,
University of Central Florida,
PO Box 162450, Orlando,
FL 32816-2450,
USA
Tel.: (407) 660-2552
Fax: (407) 875-1161
E-mail: *hobbscm@cdm.com*

Seungkwan Hong
Civil and Environmental Engineering Department,
Korea University,
1, 5-ka, Anam-dong, Sungbuk-ku
Seoul, 136-701,
Korea

INTRODUCTION

The use of membrane technology in drinking water treatment has increased dramatically in recent years (AWWA 1999; Van Der Bruggen *et al.* 2003). Membrane separation processes, such as reverse osmosis (RO) and nanofiltration (NF), are becoming more popular for several reasons, some of which include their ability to produce a superior quality of water, to reduce the size of the treatment facilities, and to simplify water treatment processes (Taylor & Jacobs 1996; Wilbert *et al.* 1993). The declining quality of source waters and increasingly stringent drinking water standards are further expanding the utilization of these treatment alternatives in full-scale water utilities (Beverly *et al.* 2000; Taylor & Hong 2000).

Operational problems, such as membrane fouling have hampered the acceptance of RO and NF technologies as a treatment of choice for low quality source waters (Hong & Elimelech 1997). Source waters with high fouling potentials require extensive feed water pretreatment to maintain membrane productivity (Taylor & Jacobs 1996). In addition, frequent chemical cleaning is often required to remove foulants adsorbed onto the surface of the membrane (Li & Elimelech 2004). Despite rigorous pretreatment and cleaning, membranes often suffer irreversible losses in productivity. Irreversible fouling results in the gradual deterioration of membrane performance and will inevitably lead to the replacement of the membrane elements in the system.

In order to minimize the costs associated with fouling control and membrane replacement, it is of paramount importance to select RO and NF membranes that possess properties that inherently resist fouling. Membrane surface

doi: 10.2166/aqua.2006.038

characteristics, regardless of fouling types, are major factors affecting the rate and extent of membrane fouling. Among such factors are surface roughness (Elimelech *et al.* 1997; Vrijenhoek *et al.* 2001; Hoek *et al.* 2003; Myung *et al.* 2005; Zhao *et al.* 2005), charge (Hong & Elimelech 1997; Childress & Elimelech 2000; Zhan *et al.* 2004; Myung *et al.* 2005; Wang *et al.* 2005) and hydrophobicity (Jucker & Clark 1994; Nilson & DiGiano 1996; Cho *et al.* 2002; Laine *et al.* 2003) for RO and NF membranes. Presently, the selection of new or replacement membranes for full-scale membrane water treatment facilities is typically based on either bench-scale or pilot scale evaluation of several membranes commercially available at the time of testing (Fu *et al.* 1994). A more fundamental approach, based on membrane surface properties, is not commonly explored for the selection of membranes. In order to achieve this goal, a correlation between membrane properties and membrane fouling potential must be established.

In this study, RO/NF membrane film characteristics were characterized using atomic force microscopy (AFM) for surface roughness, streaming potential analysis (SPA) for surface charge, and contact angle measurements for hydrophobicity. These characteristics were then related to membrane productivity as determined from flat sheet tests using a high organic groundwater taken from a surficial aquifer that served as the drinking water source for the City of Plantation, Florida. The impact of surface properties on membrane performance was assessed using these results.

MATERIALS AND METHODS

Source water quality

The source water used in this study was an organic rich groundwater used by the City of Plantation's Central Water Treatment Facility, a 45,400 $m^3\,day^{-1}$ (12 − mgd) membrane softening plant located in south Florida. This water originated from the surficial Biscayne Aquifer and had very consistent water quality year-round. The pH of this water was near neutral, and both hardness and alkalinity values were high. Both iron and total organic carbon values were relatively high at approximately 1.5 $mg\,l^{-1}$ and 22 $mg\,l^{-1}$, respectively. Finally, the temperature of this water was typical of south Floridian groundwaters, measuring 25°C (77°F).

Water samples were collected from the City of Plantation's Central Water Facility on 28 July 1999 for testing purposes. These samples were taken from one of eight wells that feed the Central Water Facility with water from the Biscayne Aquifer. These samples were immediately analysed to determine a host of water quality parameters. The average values of the measured parameters followed relatively closely to the values reported by the utility, as shown in Table 1, with few exceptions. Both the measured pH and total dissolved solids values of the samples averaged slightly higher, at 7.9 and 427 $mg\,l^{-1}$, respectively, than the reported values of 7.1–7.2 and 349 $mg\,l^{-1}$. Total organic carbon measured slightly less than the value reported by the utility at 17.5 $mg\,l^{-1}$. Hardness and alkalinity values of 333 $mg\,l^{-1}$ as $CaCO_3$ and 281 $mg\,l^{-1}$ as $CaCO_3$, respectively, agreed very well with the reported values of 307 $mg\,l^{-1}$ as $CaCO_3$ and 276 $mg\,l^{-1}$ as $CaCO_3$.

The molecular weight distribution of the natural organic matter (NOM) present in the source water was determined by high performance liquid chromatography-size exclusion chromatography (HPLC-SEC, Waters) with a protein-pak column and a 20 μl sample loop (Shimadzu) (Amy *et al.* 1992), which allowed a separation range of 1.0–30.0 kDa. The lower detection limit of 58 Da was identified and verified using an acetone solution. Standards for the molecular weight calibration curve were prepared with sodium polystyrene

Table 1 | Plantation City source water quality

Parameter	Annual average	Measured values*
pH	7.2	7.9
TDS ($mg\,l^{-1}$)	349	427
Hardness ($mg\,l^{-1}$ as $CaCO_3$)	307	333
Alkalinity ($mg\,l^{-1}$ as $CaCO_3$)	276	281
Iron ($mg\,l^{-1}$)	1.5	N/A
Turbidity (NTU)	N/A	3.4
TOC ($mg\,l^{-1}$)	22	17.5
Temperature (°C)	25	20**

*Water sample was collected on 28 July 1999.
**Temperature at which fouling studies were conducted.

sulfonate (0.25, 1.8, 4.6 and 8.0 kDa) with the lower range values confirmed by acetone and salicylic acid solutions, with molecular weights of 58 and 138 Da, respectively.

The structure (hydrophobicity, transphilicity and hydrophilicity) of the organic matter was resolved through fractionation (Aiken *et al.* 1992). XAD-8 and XAD-4 resins (Rohm and Haas, Philadelphia, Pennsylvania) were used for NOM fractionation into hydrophobic NOM (XAD-8 adsorbable), transphilic NOM (XAD-4 adsorbable), and hydrophilic NOM (neither XAD-8 nor XAD-4 adsorbable) components. Clean resins were transferred to a resin column and subsequently rinsed with 0.1 N NaOH and HCl solutions until the dissolved organic carbon measurements of the column effluent were identical to the measurements of the distilled water (Milli-Q) used to prepare the solutions. Prior to fractionation, all samples were filtered with a 0.45 μm filter and acidified to pH ≤ 2 with 5 N HCl. NOM fractions adsorbed to the resins were eluted by passing a 0.1 N NaOH solution through each column. Mass fractions of each NOM component were then determined through dissolved organic carbon measurements of each eluted solution and the XAD-8/4 effluent.

Lastly, the charge density of the organic matter was determined through a potentiometric micro-titration. An autotitrator (Metrohm 702SM Titrino, Switzerland), capable of titration increments of 0.025 ml, was used in conjunction with a pH meter (Fisher Scientific) and probe (8104BN, Orion) to perform all titrations. Prior to titration, all inorganic carbon species were removed by acidification to pH ≤ 3 with 5 N HCl and nitrogen gas sparging. Data were gathered and titration curves were plotted such that carboxylic and phenolic acidity could be determined.

RO/NF membranes

The BW-30FR (Dow-FilmTec), LFC-1 (Hydranautics) and X-20 (Trisep), were the tested RO membranes, and the NF-70 (Dow-FilmTec), TFC-ULP (Koch-Fluid System) and HL (Osmonics) were the tested NF membranes in this study. The manufacturer stated water mass transfer coefficients (MTCs) of the RO membranes were 0.0123 to 0.0369 lmh/kPa (0.05 to 0.15 gfd/psi), and were considered to be low pressure RO membranes. The manufacturer MTCs for the NF membranes ranged from 0.0492 to 0.1723 lmh/kPa (0.2 to 0.7 gfd/psi).

Membrane filtration unit

The membrane filtration unit consisted of two identical, low foulant, stainless steel test cells (Sepa CF, Osmonics Inc.) operated in parallel and with both feed and permeate spacers. Each cell had channel dimensions of 14.5 cm (5.7 in) in length, 9.4 cm (3.7 in) in width, and 0.86 mm (0.034 in) in height, which provided an effective membrane area of 1.361×10^{-2} m^2 (21.1 in^2). The feed solution for these cells was contained in a 20 l (5 gal) HDPE Nalgene Cylindrical Tank and was mechanically agitated by a magnetic stirring plate. The temperature of the feed solution was maintained at 20°C (68°F) by a stainless steel heat exchange coil used in conjunction with a refrigerated recirculator (Neslab CFT-33). The solution was pumped out of the reservoir and pressurized by a Hydracell pump (Wanner Engineering), which was capable of delivering 4.2 lpm (1.1 gpm) at a maximum pressure of 3.4 MPa (500 psi). The concentrate flow (crossflow velocity) was monitored via a floating disk flowmeter (Blue White Industries) and could be adjusted by a by-pass valve (Swagelok). The feed pressure was manipulated through a back pressure regulator (US Paraplate) located immediately downstream of the test cell concentrate exit. Through careful adjustment of the by-pass valve and the back pressure regulator, the crossflow velocity and feed pressure could be finely controlled. The permeate flow, operation time and cumulative volume of permeate were continuously monitored and recorded by two digital flowmeters (Humonics) interfaced with two Dell PCs.

Membrane filtration experiments

The fouling behaviour of each membrane was assessed through bench-scale filtration experiments. Prior to fouling experiments, the membrane filtration unit was cleaned thoroughly using sodium dodecyl sulphate and sodium laurel sulphate (SDS and SLS), sodium hydroxide and citric acid solutions. The membrane sections were then placed in each test cell and sealed via a hydraulic press, per manufacturer instructions. All filtration studies were preceded by a stabilization period in which the membranes were equilibrated with deionized (DI) water, which contained 10^{-3} M $NaHCO_3$ (pH ≈ 7.9), for 18–24 h, at a

pressure that produced the predetermined initial flux e.g. 29 lmh (17 gfd). After stabilization, the test unit was flushed with 2 l (0.5 gallons) of the testing solution to remove the sodium bicarbonate solution from the hold-up volume. The membranes were then evaluated for the ensuing 48 h with 18 l (4.5 gallons) of the testing solution at an initial flux of 29 lmh (17 gfd). Variations in permeate flux were monitored and plotted against operation time in order to assess the performance of the membranes.

The selectivity of each membrane was also evaluated for each fouling experiment. At the beginning of each fouling test, both feed and permeate samples were collected for TDS and TOC analyses. The conductance of both the feed and permeate streams were measured with a conductance meter (Model 32, YSI) and converted to TDS through the Russell and Langelier approximations presented in Equations 1 and 2 below (Snoeyink & Jenkins 1980). Similarly, TOC data were obtained through the use of a TOC analyser (Phoenix 8000 UV-Persulphate Analyser, Dohrmann).

$$\mu = 1.6 \times 10^{-5} \times (Conductance) \quad (1)$$

$$TDS = \frac{\mu}{2.5 \times 10^{-5}} \quad (2)$$

where: μ = ionic strength; conductance in micromhos per centimetre

Membrane surface characterization

In order to correlate fouling potential to membrane surface properties, the selected RO/NF membranes were thoroughly characterized prior to fouling experiments. The surface roughness was first characterized by atomic force microscopy (AFM) and by scanning electron microscopy (SEM). Furthermore, indicators of membrane surface charge and hydrophobicity were determined through streaming potential analysis (SPA) and contact angle measurements, respectively.

The Digital Instruments (DI) NanoScope™ was selected to analyse the surface roughness for all membrane samples. In order to minimize sample damage and maximize resolution, the DI AFM was operated in tapping mode. This mode operated by scanning a tip, attached to the end of an oscillating cantilever, across the surface of the sample, which resulted in the 'tapping' of the tip on the surface of the sample. The vertical position of the scanner at each (x, y) data point was stored by the computer, which formed a topographic image of the sample surface. In addition, the computer analysed these data, which made it possible to determine a host of parameters, including average roughness and 3-dimensional surface area. In order to ensure representative data, a total of three scans were performed for each membrane, each on a separate membrane section. These data were then tabulated, averaged and analysed to evaluate membrane surface roughness. In addition, SEM photographs (JOEL 6400F Scanning Electron Microscope) were taken of each membrane.

The zeta potential of the membrane surface at the plane of shear was determined using a streaming potential analyser (BI-EKA, Brookhaven Instruments Co.). The zeta potential was calculated from the streaming potential by the relationship presented in Equation 3 (McFadyen 2002). Additional details regarding the development of this relationship can be found elsewhere (McFadyen 2002).

$$\zeta = \frac{V_s}{\Delta p} \frac{\eta}{\varepsilon \varepsilon_0} \frac{L}{A} \frac{1}{R} \quad (3)$$

where: ζ = zeta potential
V_s = streaming potential
Δp = hydrodynamic pressure difference
η = liquid viscosity
ε = liquid permittivity
ε_0 = permittivity of the free space
L = sample length
A = sample cross-sectional area
R = electrical resistance

All measurements were performed at room temperature, approximately 22°C (72°F), with a background electrolyte solution of 10^{-2} M NaCl. Furthermore, to avoid ionic interference, the acid and base legs (referenced to the initial pH) were titrated with separate membrane samples in order to generate a zeta potential curve from pH 3 to 11. Two separate tests were performed for each membrane, and trend lines were developed using the best-fit logarithmic model for both tests, using Microsoft Excel.

The contact angle measurements were obtained through the captive or adhering bubble technique (Goniometer,

Rame-Hart). Unlike the sessile drop technique, this technique allowed for the determination of the contact angle in an aqueous phase. In order to complete these measurements, each membrane sample was mounted on a flat surface with the active layer exposed. The assembly was then inverted, and lowered into a quartz cell, which contained DI water, such that the active layer of the membrane was face down. A submerged syringe with a U-shaped needle attachment delivered a bubble, of pre-determined size, which floated up to the membrane surface. Once the air bubble stabilized with the surface of the membrane, the contact angle on each side of the bubble was measured by an automated goniometer. In order to ensure representative results, a total of six contact angle measurements were made for each membrane.

RESULTS AND DISCUSSION

Organic analysis

The molecular weight distribution of the dissolved organic material or natural organic matter (NOM) in the City of Plantation raw water is presented in Figure 1. As shown, a significant portion of the organic matter was high in molecular weight (above 1,000 g mol^{-1}). The results obtained from the fractionation onto XAD 8/4 resins revealed that the majority (54.9%) of the organic matter was hydrophobic in nature as presented in Figure 2, which may suggest a greater propensity for organic fouling.

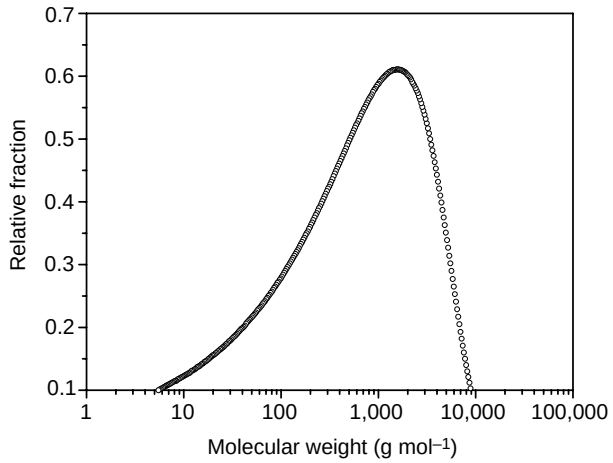

Figure 1 | Natural organic matter size distribution for the City of Plantation's surficial groundwater.

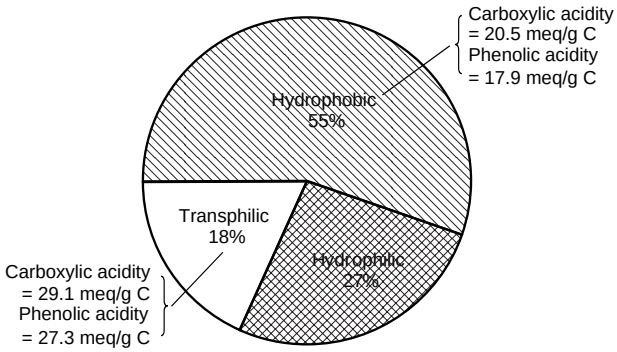

Figure 2 | Natural organic matter structure and functionality for the City of Plantation's surficial groundwater.

Bench-scale membrane performance

The fouling behaviour of selected RO/NF membranes was first investigated via bench-scale filtration experiments using the highly organic ground water used by the membrane softening plant at the City of Plantation, Florida. Figure 3 shows permeate flux versus operation time for RO and NF membranes tested, and it should be noted that the permeate flux shown in this figure was the average flux for two fouling test runs. While all membranes suffered a loss of flux, the severity of membrane fouling was different among membranes. The order of RO membranes in increasing fouling rate was LFC-1, BW-30FR, and X-20; while the order of NF membranes in increasing fouling rate was HL, TFC-ULP, and NF-70. The initial MTCs as determined by flat sheet testing were the same as specified in the literature by manufacturer, which indicated these tests were representative of the membrane films used in the commercially available elements.

The TOC and TDS selectivity of each membrane is shown in Table 2, and was evaluated to further verify that the membrane samples were representative of the film in the commercially available elements. As expected, all RO membranes rejected more TDS and TOC than did NF membranes. The higher RO rejection was generally attributed to the 'tightness' of RO membranes, as shown by corresponding lower MTC values.

Surface roughness

In general, the roughness of any surface is dependent on the size, shape, frequency and distribution of the surface

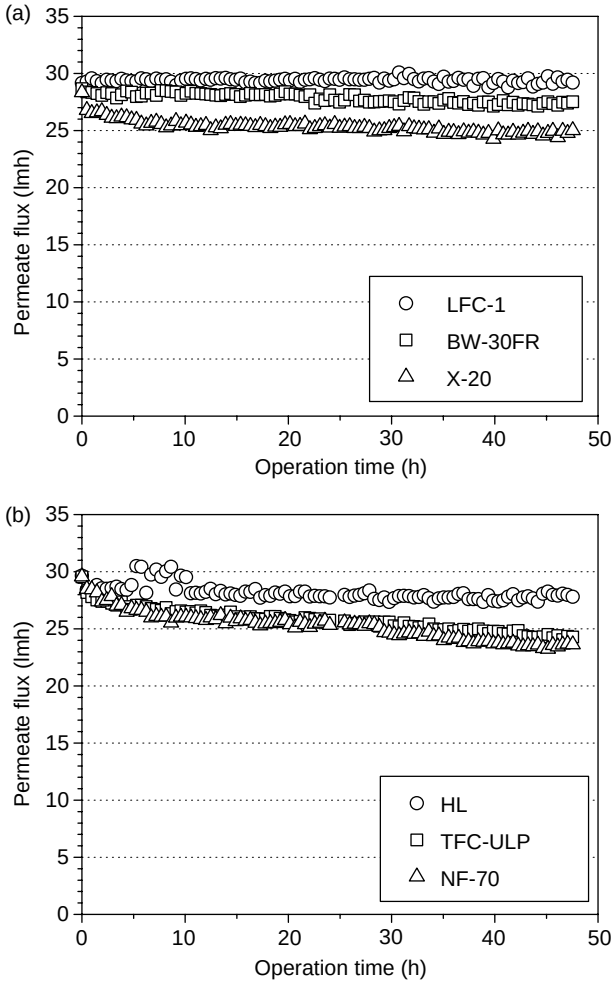

Figure 3 | Flux variations with respect to filtration time: (a) RO and (b) NF.

projections. An atomic force microscope was chosen and utilized for the analysis of surface peaks on the RO and NF membranes. This particular instrument was selected for its ability to resolve extremely small surface features, on the order of several nanometres. While AFMs are capable of analysing a host of descriptive parameters, two criteria were used to quantify membrane surface roughness, average roughness with the associated root mean square, and the surface area difference. The average roughness denotes the arithmetic average of the absolute values of the surface height deviations measured from the centre plane. The root mean square roughness is the standard deviation of the average roughness. The surface area difference represents the percentage increase of the three-dimensional surface area over the two-dimensional surface area, which accounts for both the magnitude and the frequency of surface features, and provides a good measure of surface roughness.

The AFM scans of the selected membranes are presented in Figure 4. The majority of the membranes showed a surface that was covered with 'mountainous peaks'. Visual inspection of the SEM images revealed similar surface features and were in a good agreement with the AFM scans for all of the membranes tested. The statistical analyses of the surfaces of the membranes, as determined by the AFM, are summarized in Table 3. For the six different RO/NF membranes analysed, the average roughness ranged from 10.1 to 56.7 nm. The order of increasing average membrane roughness of RO membranes was X-20, LFC-1 and BW-30FR. The order of

Table 2 | Summary of bench-scale membrane performance tests

Membrane	Type	Initial MTC (lmh/kPa)	Flux decline ratio (%)*	TDS rejection (%)	TOC rejection (%)
BW-30FR	RO	0.0271 (0.11 gpd/psi)	4.4	98.0	98.1
LFC-1		0.0320 (0.13 gfd/psi)	0.0	98.7	98.0
X-20		0.0246 (0.10 gfd/psi)	12.6	97.2	97.8
HL	NF	0.0836 (0.34 gfd/psi)	6.1	57.7	94.6
NF-70		0.1476 (0.60 gfd/psi)	20.1	43.3	71.0
TFC-ULP		0.0590 (0.24 gfd/psi)	17.6	86.9	95.6

*Flux decline ratio = (initial flux − final flux)/initial flux × 100 (%).

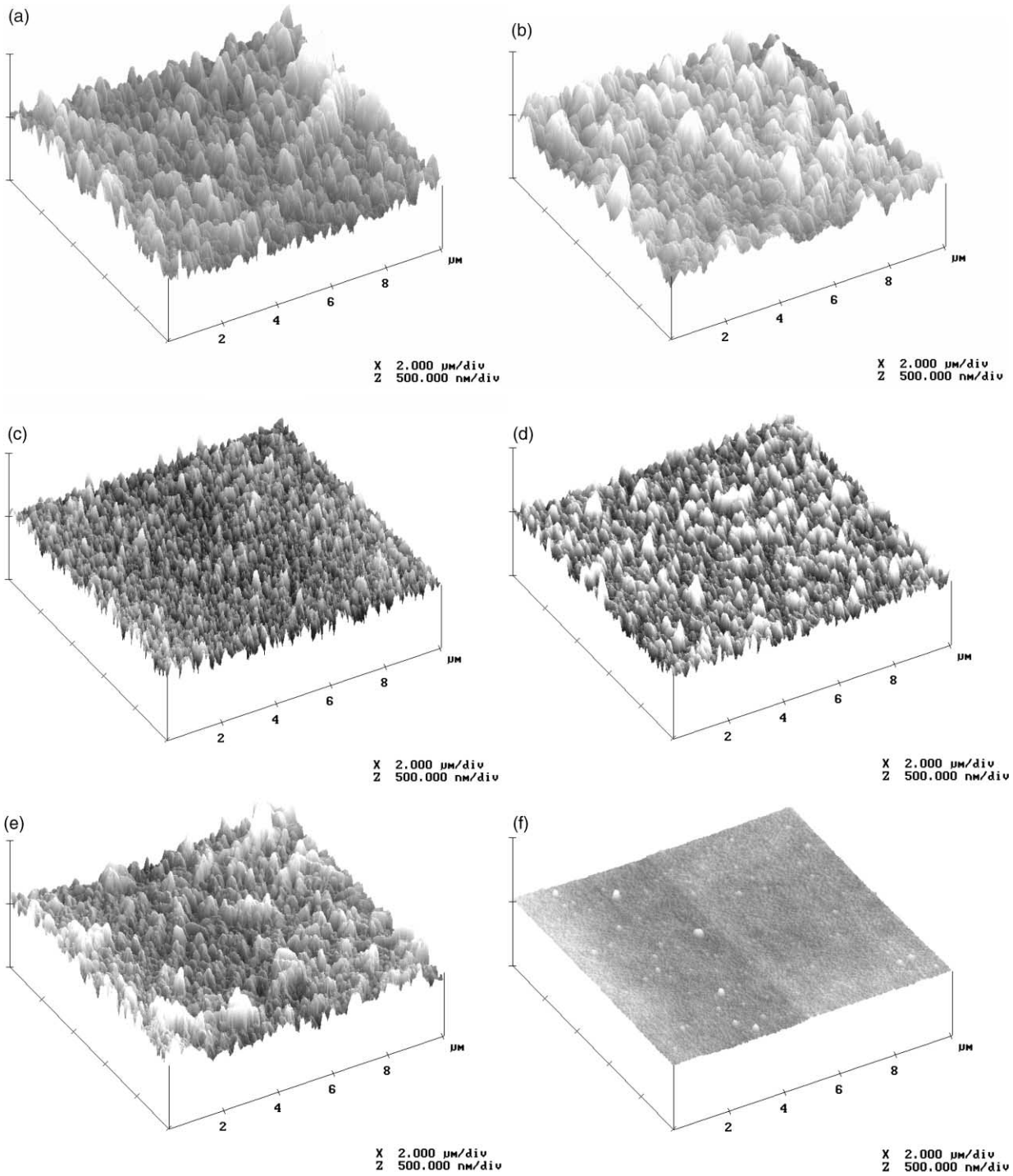

Figure 4 | AFM Images of RO and NF Membranes: (a) BW30-FR, (b) LFC-1, (c) X-20, (d) TFC-ULP, (e) NF-70 and (f) HL.

increasing average membrane roughness of NF membranes was HL, TFC-ULP and NF-70. The surface area difference for these membranes ranged from 1.2 to 32.7%. The order of increasing surface area difference for RO membranes was LFC-1, BW-30FR and X-20; and HL, TFC-ULP, and NF-70 for NF membranes.

It is important to understand the difference between average roughness and surface area difference when

Table 3 | Summary of membrane surface characteristics

Membrane	Type	Average roughness (nm)	Surface area difference (%)	Zeta potential (mV)*	Contact angle (°)
BW-30FR	RO	56.7 ± 73.2	25.8 ± 0.2	−6.0	55.3 ± 1.2
LFC-1		52.0 ± 67.4	16.90 ± 2.7	−5.4	51.7 ± 1.0
X-20		33.4 ± 41.6	32.7 ± 6.6	−15.0	54.1 ± 1.3
HL	NF	10.1 ± 12.8	1.2 ± 0.2	−7.9	51.9 ± 1.0
NF-70		43.3 ± 56.5	20.7 ± 1.3	−8.3	52.5 ± 0.9
TFC-ULP		30.6 ± 38.9	18.0 ± 1.1	−10.2	51.9 ± 5.3

*Zeta potential was calculated at pH 7.9 using trend lines developed.

assessing the roughness of a membrane surface. Depending on the frequency and distribution of surface projections, these parameters can give very different results for the surface roughness. For example, the LFC-1 membrane had an average roughness of 52.0 ± 67.4 nm, as shown in Table 3, and had the second highest average roughness of the RO membranes tested. However, owing to few peak counts, LFC-1 exhibited only 16.9% surface area difference, the lowest surface area difference measured for the RO membranes tested. The X-20 membrane, on the other hand, possessed numerous smaller peaks averaging 33.4 ± 41.6 nm (Table 3) and had the lowest average roughness of the RO membranes tested. Due to the high peak frequency, the surface area difference of the X-20 membrane was 32.7%, the highest surface area difference measured for the RO membranes tested. While an increase in peak count may not significantly affect the average roughness, it can dramatically increase the surface area difference, as was the case with X-20.

Surface charge

RO and NF membranes often acquire a charge on their surface when brought into contact with an aqueous solution. The surface charge was quantified by assessing the zeta potential at the plane of shear from the measured streaming potential using the Helmholtz-Smoluchowski relationship. The zeta potentials of the selected membranes were measured at various solution pHs and their results are presented in Figure 5. The experimental results clearly

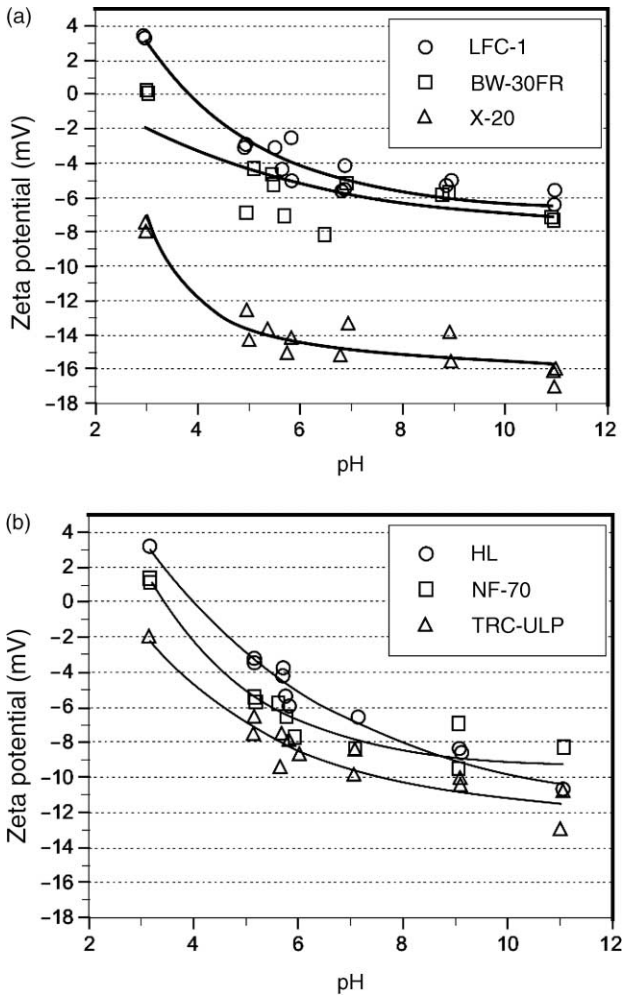

Figure 5 | Zeta potential measurements at various pH values: (a) RO and (b) NF.

demonstrate that the zeta potential of each membrane becomes more negative as the value of pH increases, which is consistent with previous investigations (Nyström *et al.* 1995). This trend arises in thin-film composite membranes from the dissociation of various functional groups (typically carboxyl) located on the surface of the membrane with increasing pH and pendant amino groups (Childress & Elimelech 1996). The zeta potential of the membranes at a pH value of 7.9 (i.e. pH of Plantation City groundwater) ranged from −5.4 to −15.0 mV, based on the exponential trend lines developed under the given solution chemistry (Table 3). The membranes in order of increasing magnitude of surface charge are LFC-1, BW-30FR and X-20 for RO membranes and HL, NF-70 and TFC-ULP for NF membranes.

Hydrophobicity

Contact angle measurements are often utilized as an indication of the hydrophobicity of a membrane surface. The origin of contact angles lies in the interactions between the solid–liquid, solid–gas and liquid–gas interfaces. The difference between the attractive forces of molecules in each phase and the attractive forces between neighbouring phases results in an interfacial energy. The distribution of this energy causes one fluid to contract, which results in the formation of the contact angle (Gourley *et al.* 1994; Marmur 1996). Figure 6 and Table 3 show the results of the contact angle measurements for each of the six selected membranes. The contact angle of the membranes were within a narrow range of 51.7° to 55.3°. Based on accepted interpretations of contact angle measurements, all six RO/NF membranes tested were hydrophilic (contact angles between 0° and 90°), with varying degrees of hydrophobicity. The membranes in order of increasing membrane hydrophobicity were LFC-1, X-20 and BW-30FR for the RO membranes and HL, TFC-ULP and NF-70 for the NF membranes.

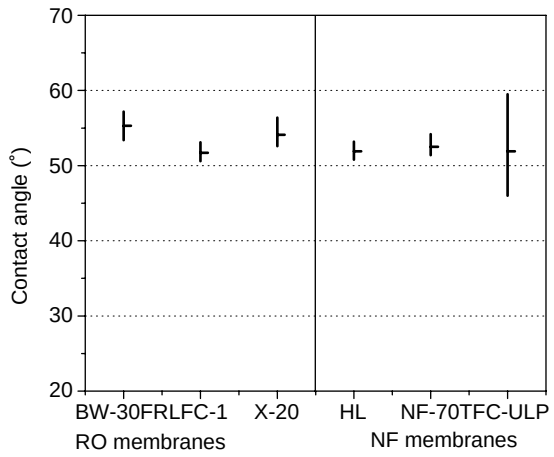

Figure 6 | Contact angle measurements of RO and NF membranes.

Correlation between surface properties and fouling

The effects of surface roughness on membrane fouling are graphically presented in Figures 7 and 8. The data presented in Figure 7 showed a reasonable visual correlation between average roughness and flux decline ratio for the NF

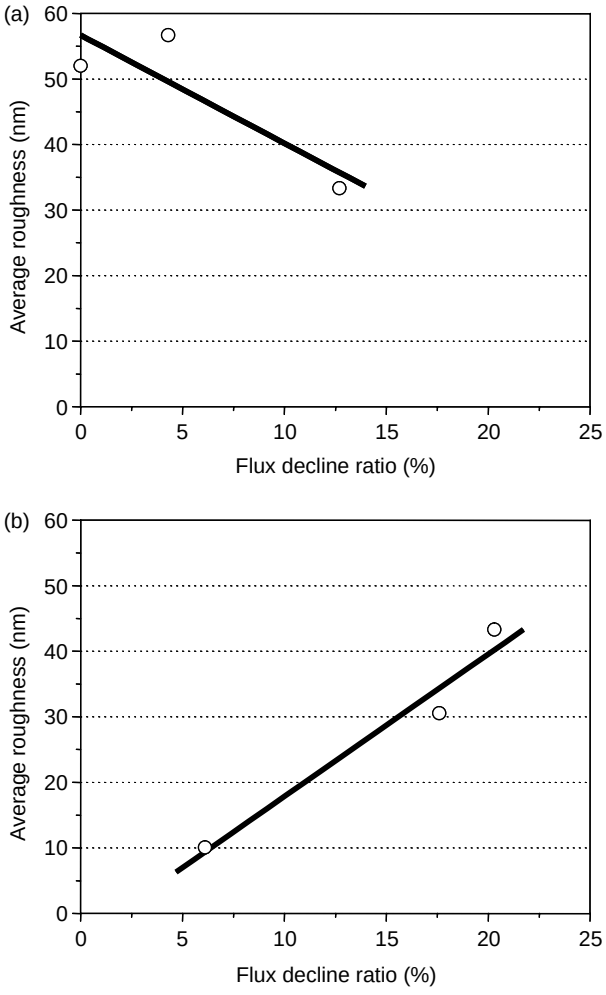

Figure 7 | Correlation between average surface roughness and flux decline ratio: (a) RO and (b) NF.

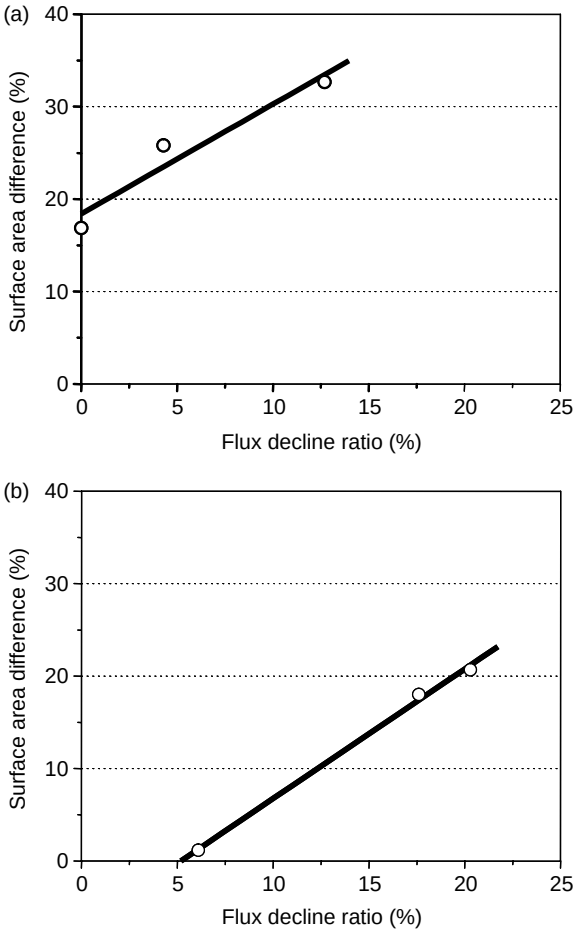

Figure 8 | Correlation between surface area difference and flux decline ratio: (a) RO and (b) NF.

membranes. However, the flux decline ratio for the RO membranes was not visually well correlated to average roughness. Plots of surface area difference versus flux decline ratio appear visually related as shown by the consistent positive slopes for both RO and NF membranes as shown in Figure 8. Although there is not adequate data for statistical interpretation, the R^2 (also known as the square of the Pearson product moment correlation coefficient and an interpretation of the proportion of the variance in the dependent variable that is attributable to the variance in the independent variable) shown in Table 4 provides a relative comparison of the relationships between surface area difference and flux decline ratio, and average roughness and flux decline ratio. The R^2 in Table 4 show that the flux decline ratio is more dependent on surface area difference than average roughness. More specifically, X-20 with a smaller average roughness suffered more flux decline than LFC-1, because it had more surface features and thus more surface area. These findings, combined with source water quality data indicating high organic content, suggest that the surface area difference is a superior indicator for organic fouling than average roughness, because only surface area difference accounts for increased surface area, which is available for adsorption.

In addition to surface roughness, membrane surface charge and hydrophobicity values were plotted against the corresponding flux decline ratios. The results revealed that both parameters were poorly related to flux decline ratio for the given experimental conditions. Specifically, there was no clear trend observed for the NF membranes investigated. Furthermore, an inverse relationship between zeta potential and flux decline ratio was even noted for the RO membranes although the correlation coefficient was relatively low. This finding may indicate that the source water tested was composed of a multitude of foulants with various electrokinetic properties. No clear correlation was established between the contact angle (i.e. hydrophobicity) and flux decline ratio. This is not surprising since the range of

Table 4 | Summary of statistical analyses

Membrane type	Statistical parameter	Average roughness	Surface area difference	Zeta potential	Contact angle
NF	R^2	0.952	0.998	0.246	0.407
	P-Value	0.140	0.026	0.670	0.560
RO	R^2	0.733	0.941	0.915	0.266
	P-Value	0.346	0.156	0.188	0.655

membrane hydrophobicity studied was very narrow, which hindered the development of any discernable trends (refer to Figure 6). Poor correlation of charge and hydrophobicity with membrane fouling suggest that surface roughness plays a dominant role in the initial stage of membrane fouling relative to other surface properties. Similar results were also observed in a study conducted by Vrijenhoek *et al.* (2001) who investigated the mechanisms of colloidal fouling using similar membranes. The lack of correlation with charge and hydrophobicity can be attributed to the degree of ionization of the film surface and organic foulants in the bulk water. Natural organic solutes could well adsorb onto the surface and increase resistance of the mass transfer of water though the film, which would appear independent of charge.

CONCLUSIONS

During RO/NF filtration of a high organic surficial groundwater, membrane fouling clearly increased with increasing surface roughness, as measured by the surface area difference. Based on visual correlations and relative statistical analyses utilizing R^2 and probability values (also known as *P*-values, which represent the probability of samples that could have been drawn from test populations assuming the null hypothesis was true), it was determined that this parameter provided a better indicator of fouling potential especially for organic adsorption than average surface roughness which is normally used to represent surface roughness, because of its inherent inclusion of both magnitude and frequency of peaks. Membrane charge and hydrophobicity were, on the other hand, loosely related to permeate flux decline, suggesting that surface roughness is a dominating factor affecting initial fouling rate.

ACKNOWLEDGEMENTS

The authors would like to extend their sincere gratitude to the American Water Works Association Research Foundation (AWWARF) for financial support. We also thank the City of Plantation's Central Water Treatment Facility, for the assistance in gathering both the operating data and source water from the Central Plant. Finally, the Advanced Material Processing and Analysis Center (AMPAC) at University of Central Florida, and Dr Amy Childress at University of Nevada, Reno, are acknowledged for membrane surface characterization. Their expertise and effort were truly valuable for this study and were greatly appreciated.

REFERENCES

Aiken, G., McKnight, D., Thorn, K. & Thurman, E. 1992 Isolation of hydrophilic organic acids from water using nonionic macroporous resins. *Org. Geochem.* **18**(4), 567–573.

Amy, G., Sierka, R., Bedessem, J., Price, D. & Tan, L. 1992 Molecular size distributions of dissolved organic matter. *J. Am. Wat. Wks Assoc.* **84**(6), 67–75.

AWWA (American Water Works Association) 1999 *Reverse Osmosis and Nanofiltration: Manual*. AWWA, Denver, Colorado.

Beverly, S., Seal, S. & Hong, S. 2000 Identification of surface chemical functional groups correlated to failure of reverse osmosis polymeric membranes. *J. Vacuum Sci. Technol.* **18**(4), 1107–1113.

Childress, A. & Elimelech, M. 1996 Effect of solution chemistry on the surface charge of polymeric reverse osmosis and nanofiltration membranes. *J. Membrane Sci.* **119**, 253–268.

Childress, A. & Elimelech, M. 2000 Relating nanofiltration membrane performance to membrane charge characteristics. *Environ. Sci. Technol.* **34**, 3710–3716.

Cho, J., Sohn, J., Choi, H., Kim, I. & Amy, G. 2002 Effects of molecular weight cutoff, f/k ratio (a hydrodynamic condition), and hydrophobic interactions on natural organic matter rejection and fouling in membranes. *J. Wat. Suppl.: Res. and Technol. – AQUA* **51**(2), 109–123.

Elimelech, M., Zhu, X., Childress, A. & Hong, S. 1997 Role of surface morphology in colloidal fouling of cellulose acetate and composite polyamide RO membranes. *J. Membrane Sci.* **127**, 101–109.

Fu, P., Ruiz, H., Thompson, K. & Spangenberg, C. 1994 Selecting membranes for removing NOM and DBP precursors. *J. Am. Wat. Wks Assoc.* **86**(12), 55–72.

Gourley, L., Britten, M., Gauthier, S. F. & Pouliot, Y. 1994 Characterization of adsorptive fouling on ultrafiltration membranes by peptides mixtures using contact angle measurements. *J. Membrane Sci.* **97**, 283–289.

Hoek, E., Bhattacharjee, S. & Elimelech, M. 2003 Effect of membrane surface roughness on colloid-membrane DLVO interactions. *Langmuir* **19**(11), 4836–4847.

Hong, S. & Elimelech, M. 1997 Chemical and physical aspects of natural organic matter (NOM) fouling of nanofiltration membranes. *J. Membrane Sci.* **132**, 159–181.

Jucker, C. & Clark, M. 1994 Adsorption of aquatic humic substances on hydrophobic ultrafiltration membranes. *J. Membrane Sci.* **97**, 37–52.

Laine, J., Campos, C., Baudin, I. & Janex, M. 2003 Understanding membrane fouling: A review of over a decade of research. *Wat. Sci. Technol.* **3**(5–6), 155–164.

Li, Q. & Elimelech, M. 2004 Organic fouling and chemical cleaning of nanofiltration membranes: measurements and mechanisms. *Environ. Sci. Technol.* **38**(17), 4683–4693.

Marmur, A. 1996 Equilibrium contact angles: theory and measurement. *Colloid Surface* **116**, 55–61.

McFadyen, P. 2002 *Zeta Potential of Macroscopic Surfaces from Streaming Potential Measurements*. Brookhaven Instruments Limited, New York.

Myung, S., Choi, I., Lee, S., Kim, I. & Lee, K. 2005 Use of fouling resistant nanofiltration and reverse osmosis membranes for dyeing wastewater effluent treatment. *Wat. Sci. Technol.* **51**(6–7), 159–164.

Nilson, J. & DiGiano, F. 1996 Influence of NOM composition on nanofiltration. *J. Am. Wat. Wks Assoc.* **88**(5), 53–66.

Nyström, M., Kaipia, L. & Luque, S. 1995 Fouling and retention of nanofiltration membranes. *J. Membrane Sci.* **98**, 249–262.

Snoeyink, V. & Jenkins, D. 1980 *Water Chemistry*. John Wiley & Sons, New York.

Taylor, J. & Hong, S. 2000 Potable water quality and membrane technology. *J. Lab. Med.* **31**(10), 563–568.

Taylor, J. & Jacobs, E. 1996 Reverse osmosis and nanofiltration. In: Mallevaille, J., Odendaal, P. E. & Wiesner, M. R. (eds) *Water Treatment: Membrane Processes*. American Water Works Association Research Foundation, McGraw Hill, New York.

Van Der Bruggen, B., Vandecasteele, C., Van Gestel, T., Doyen, W. & Leysen, R. 2003 A review of pressure-driven membrane processes in wastewater treatment and drinking water production. *Environ. Prog.* **22**(1), 46–56.

Vrijenhoek, E., Elimelech, M. & Hong, S. 2001 Influence of membrane surface properties on initial rate of colloidal fouling of reverse osmosis and nanofiltration membranes. *J. Membrane Sci.* **188**, 115–128.

Wang, Z., Zhao, Y., Wang, J. & Wang, S. 2005 Studies on nanofiltration membrane fouling in the treatment of water solutions containing humic acids. *Desalination* **178**(1–3), 171–178.

Wilbert, M., Leitz, F., Abart, E., Boegli, B. & Linton, K. 1993 *The Desalting and Water Treatment Membrane Manual: A Guide to Membranes for Municipal Water Treatment*. US Department of the Interior, Bureau of Reclamation, Denver, Colorado.

Zhan, J., Liu, Z., Wang, B. & Ding, F. 2004 Modification of a membrane surface charge by a low temperature plasma induced grafting reaction and its application to reduce membrane fouling. *Separation Sci. Technol.* **39**(13), 2977–2995.

Zhao, Y., Taylor, J. & Hong, S. 2005 Combined influence of membrane surface properties and feed water qualities on RO/NF mass transfer, a pilot study. *Wat. Res.* **39**(7), 1233–1244.

First received 27 January 2006; accepted in revised form 20 May 2006